ARTICLES

Picosecond time-resolved spectroscopy of the excited state in a soluble derivative of poly(phenylene vinylene): Origin of the bimolecular decay

Arthur Dogariu, Dan Vacar, and Alan J. Heeger
Institute for Polymers and Organic Solids, University of California, Santa Barbara, Santa Barbara, California 93106
(Received 17 February 1998; revised manuscript received 6 July 1998)

Picosecond time-resolved spectroscopy studies are performed on solutions and thin films of poly[2-methoxy-5-(2′-ethyl-hexyloxy)-1,4-phenylene vinylene] (MEH-PPV) in order to examine the excited state. Interactions between excitations on different chains result in bimolecular decay dynamics. Since a contribution from bimolecular decay is observed at excitation densities above 10^{18} cm^{-3}, excitations on different chains interact in the solid state within the picosecond time regime over distances of at least 10 nm. We analyze the time dependence of the interaction dynamics predicted by different models and conclude that Förster transfer makes a significant contribution to the bimolecular interaction. However, in order to explain both the magnitude of the bimolecular decay coefficient and the interaction range (at least 10 nm in the picosecond time regime), quantum delocalization well beyond a single chain must be assumed. We conclude that the wave function of the photoexcitations extends over about 5 nm. [S0163-1829(98)05140-6]

I. INTRODUCTION

Conjugated polymers offer promise as high performance materials for use in optoelectronic devices such as light-emitting diodes,[1,2] light-emitting electrochemical cells,[3] photodiodes,[4] and lasers.[5–7] While there is agreement that this class of semiconducting polymers offers promise for a variety of electronic applications, the nature of the primary photoexcitations is controversial. Estimates of the binding energy of the electron and hole in the photoexcited state (the exciton) range from 0.2 eV or less,[8,9] up to 0.9 eV.[10,11] In the case of weak binding, the exciton would be delocalized over many monomers on a given chain and, depending on the strength of the interchain transfer interaction, even over several chains; whereas a large binding energy would imply localization on a few monomers of a given chain. A second area of disagreement centers around photoluminescence (PL) quenching at high excitation densities in thin films. Initially, the formation of nonradiative interchain polarons (electron and hole on different chains) was proposed as the mechanism.[12,13] More recent studies indicate interchain exciton formation.[14,15] At moderately high excitation densities, bimolecular decay, resulting from interchain interactions between the excited species, is responsible for the fast PL decay.[16–21] At high excitation conditions, the formation of biexcitons becomes favored.[22–24]

In this paper, we present the results of a comprehensive study of the time-resolved excited-state spectroscopy of the conjugated polymer, poly[2-methoxy-5-(2′-ethyl-hexyloxy)-1,4-phenylene vinylene] (MEH-PPV) in solution and in solid films. By means of femtosecond time-resolved spectroscopy, we study the excited-state spectra (absorption, emission, and stimulated emission) and the time decay of the excited-state spectral features. At excitation densities greater than 10^{18} cm^{-3}, interactions between excitations on different chains result in bimolecular decay dynamics. We analyze the time dependence of the interaction dynamics predicted by different models and conclude that the dipole-dipole interaction, excitation diffusion, and quantum delocalization contribute to the bimolecular interaction. However, Förster energy transfer (via the dipole-dipole interaction) between localized excitations supplemented by classical diffusion cannot account for both the magnitude of the coefficient of the bimolecular decay term and the range of the interchain interaction. Quantum delocalization over distances of about 5 nm must be assumed to explain the observation that in the solid state, excitations on different chains interact within the picosecond time regime over distances of at least 10 nm.

II. EXPERIMENTAL METHODS

The samples were solutions of MEH-PPV in tetrahydrofuran (THF) or thin films spin cast onto sapphire substrates from THF. The solutions were prepared in a cuvette with 1 mm optical path length and an optical density (OD) of 0.5–1.5 at the absorption peak. The films were 500 nm thick with OD$>$2 at the absorption peak. Figure 1 shows the linear absorption (dashed line) spectrum and the PL (solid line) spectrum of the thin film samples. The PL emission is Stokes shifted with respect to the absorption, a feature that makes these conjugated polymers suitable for use in luminescence applications (e.g., as the gain material in lasers) where minimum self-absorption (reabsorption) is important.

The source for the ultrafast nonlinear spectroscopic measurements was a Spectra-Physics amplified Ti:sapphire system followed by an optical parametric amplifier (OPA). This facility provides 120 fs (full width at half maximum) pulses at a repetition rate of 1 kHz with tunable wavelength. We used the fourth harmonic of the idler from the OPA to pump

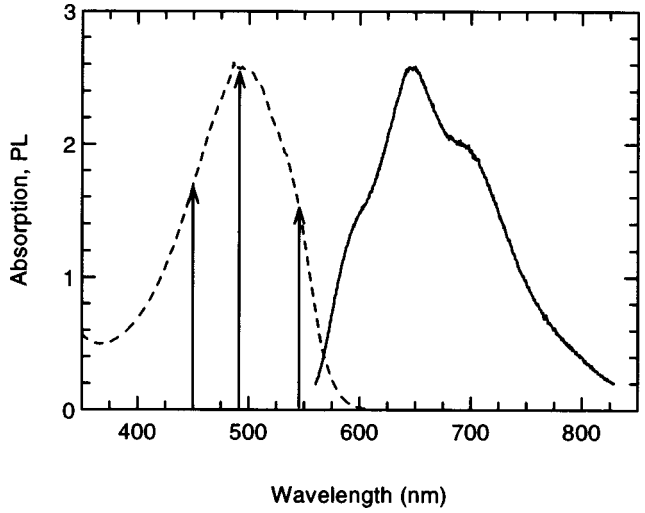

FIG. 1. Optical density (dashed line) and PL (solid line) spectra for MEH-PPV. The arrows indicate the pump wavelengths used for the data in Fig. 2.

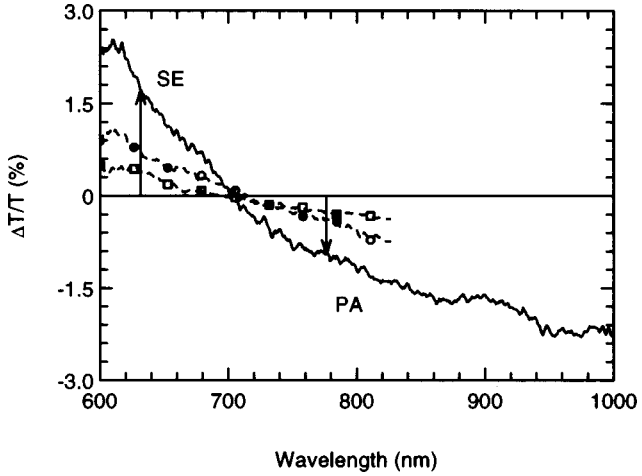

FIG. 2. The photoinduced change in transmittance spectrum ($\Delta T/T$) of a MEH-PPV film (thickness 0.5 μm) at 1 ps (solid line), 10 ps (circles), and 50 ps (squares) after the 490-nm pump. The arrows indicate the probing wavelengths for SE (632 nm) and PA (775 nm) as described in the text.

within the absorption band of MEH-PPV (450–560 nm). In order to probe the photogenerated excited state, the transmission of a femtosecond white-light continuum pulse was monitored (the continuum pulse was obtained by focusing the $\approx$1.3-μm signal beam from the OPA into a 1-mm-thick sapphire plate). In this way, we were able to probe the excited-state spectrum in a single measurement from 500 nm out to 1.1 μm (the limit of our silicon detectors). The linear chirp of the white-light continuum beam was measured to be about 80 fs for every 100 nm. The probe beam was split into two beams; one was used as a reference to normalize out fluctuations in the continuum pulse. After passing through a 0.3-m spectrometer, the beams were detected using a Peltier-cooled charge-coupled device camera. In this way, we were able to record excited-state spectra as changes in transmittance with sensitivity as low as 1%.

In order to study the time evolution of the excited state features, we performed single-wavelength measurements with much higher sensitivity. The selected wavelengths (obtained by using interference filters) are indicated in Fig. 2: 632 nm for the SE and 775 nm for the PA spectral regions. A 200-Hz mechanical chopper was placed in the pump beam, and the in-phase changes in the probe beam were detected by a lock-in amplifier. By using small integration times (30 ms) for the lock-in amplifier, we were able to follow fast changes in the probe-beam energy by normalizing to the reference beam. After averaging, we obtained a hybrid between frequency gating and shot-to-shot averaging, which allowed measurement of signals smaller than 10^{-3} (i.e., with a precision of 10^{-4}).

Care has been taken to ensure that all the data were taken on pristine, unoxidized samples. All the experiments were performed with the solid samples under a dynamic vacuum. After each scan, we checked reproducibility by recovering the signals under the same conditions while illuminating in the same spot in the sample. To prevent laser-induced damage in the sample, the input fluences were always kept one or two orders of magnitude below the measured damage thresholds.[22]

III. EXPERIMENTAL RESULTS

The time-resolved nonlinear spectrometer was used to investigate the excited-state spectral features. Figure 2 shows the differential change in the transmittance of MEH-PPV measured at 1, 10, and 50 ps after the excited state was induced by a pump pulse at 490 nm. One can easily identify the distinct regions of positive differential transmission (corresponding to gain) and negative differential transmission (corresponding to loss). In the gain region, at frequencies within the PL spectrum, the stimulated emission (SE) overcomes the photoinduced absorption (PA), whereas in the loss region, the PA dominates.

Within our resolution, we have not detected any change in the spectral shape of the excited-state spectrum as a result of varying the pump wavelength within the absorption band. Also, there was no change in spectral shape when pumping at different excitation levels. As seen in Fig. 2, the spectra decay uniformly; the excited-state spectra at 1, 10, and 50 ps after the pump pulse are similar in shape.

A. Low density dynamics

Using the high-sensitivity single-wavelength measurements, the decay of the SE and PA features were studied in solutions and films of MEH-PPV. We have previously reported[25] that the dynamics of SE and PA are insensitive to the pump wavelength within the main absorption band of MEH-PPV. Figure 3 shows the differential changes in transmittance (positive for SE probed at 632 nm and negative for PA probed at 775 nm) through (a) a 0.5-μm film, and (b), a 1-mm cell containing the solution of MEH-PPV in THF. The pump wavelength was 450 nm (triangles), 490 nm (squares), and 545 nm (circles). For these low-density studies the highest excitation density was below 2×10^{18} cm^{-3} in film, and on the order of 10^{16} cm^{-3} in solution. This ensures, as discussed in detail in Sec. III B, that the excitation density is low enough to neglect interactions.[19] Figure 3 shows that the decay of the excited state is independent of the pump photon energy (at least within the visible part of the absorption

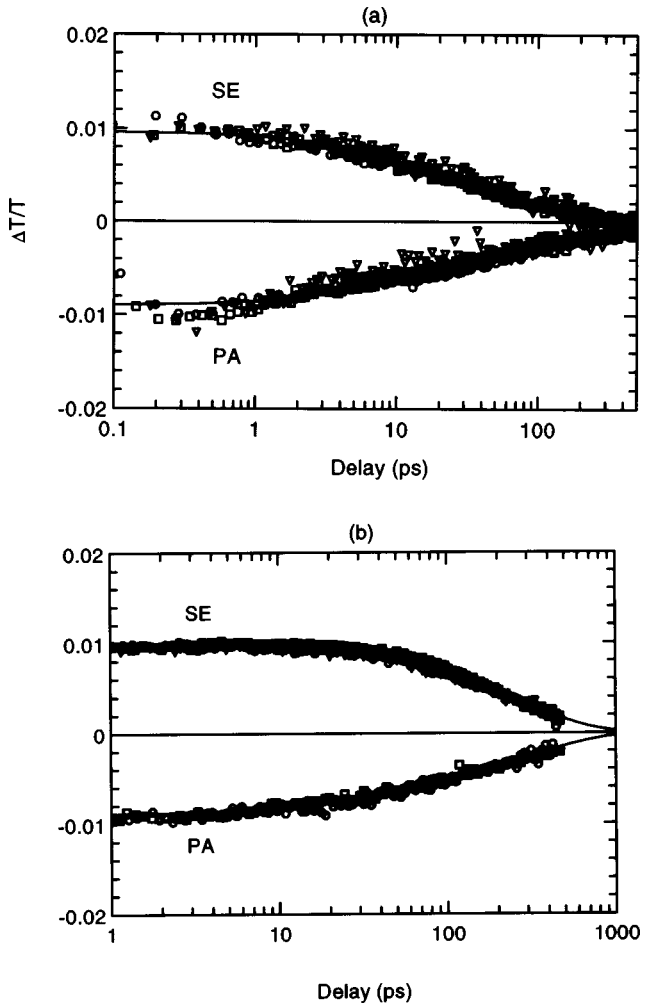

FIG. 3. Differential change in transmittance for SE at 632 nm (positive) and PA at 775 nm (negative) for a MEH-PPV film with 0.5 μm thickness (a) and 1-mm cell of solution in THF (b) when pumped at 450 nm (triangles), 490 nm (squares), and 545 nm (circles). Excitation density is below 2×10^{18} cm^{-3} in film and 10^{16} cm^{-3} in solution.

band). By comparing the results shown in Fig. 3, one sees that the lifetime of the excited state of MEH-PPV is slightly shorter in a solid film than in a solution. This is not surprising; there are additional channels for decay (e.g., through defects) in the solid state.

In Fig. 3, the lines represent fits to the SE and PA data using a dual exponential decay

$$\Delta T/T(t)=\Delta T/T(0)[b\ \exp(-t/\tau_1)+(1-b)\exp(-t/\tau_2)], \tag{1}$$

where b is the fraction of excitations that decay by the faster channel. The numbers for the decay times and the b factor obtained by fitting the data in Fig. 3 are shown in Table I. Because the differential change in transmittance is proportional to the excited state density

$$\Delta T/T=\exp\left(\int \Delta\alpha\ dz\right)\cong\sigma\int N\ dz. \tag{2}$$

Equation (1) describes the temporal evolution of the excitation density. The decay times (see Table I) are almost identical with the decay times reported by Zhang *et al.*[18] The two-exponential fit is certainly not unique, and should not be considered as fundamental. For example, a stretched exponential could be used equally well (and might have more significance in a disordered material). Even a single exponential fits reasonably well and provides a simple and convenient way to characterize the decay at low-excitation densities.

TABLE I. The short (τ_1) and long (τ_2) lifetimes and the weighting factor b used in Eq. (1) to fit the data in Fig. 3.

	b	τ_1 (ps)	τ_2 (ps)
PA solution	0.25 ± 0.03	30 ± 20	320 ± 70
SE solution			260 ± 40
PA film	0.45 ± 0.05	$15\pm\ 5$	270 ± 50
SE film	0.55 ± 0.05	$13\pm\ 3$	130 ± 30

The long decay time of the PA and the SE in solution are close to the 300-ps PL lifetime, which we measured using a time integrating gate.[26] The SE is dependent on the solvent from which the film was spin cast, implying that chain packing and film microstructure play an important role in determining the amount of radiative vs nonradiative decay of the excitations. In the optimum case, when the nonradiative decay rate is negligible, one finds that the PA and SE lifetimes are identical,[17] whereas in the opposite extreme, when the decay of the excitations is mostly nonradiative, one finds very little, if any, SE.[12,13] From Fig. 2, we conclude that the SE and PA are correlated at least between 600 and 850 nm. There is also a PA contribution from another excited state that makes the lifetimes a little different in the PA and SE even in solution, where intrachain contributions dominate. Samuel, Rumbles, and Collison[15] reported much longer lifetimes for the solid films of MEH-PPV, mainly due to long-lived interchain excitons, which lead to a strong red spectral shift of the PL. However, we did not find any significant difference between the PL or SE spectra in solution and film. Thus, the MEH-PPV films used in this study, obtained from THF solutions, have a much smaller excimer yield than films obtained from toluene.[14,15] In order to resolve the discrepancy between our SE data and the lack of SE reported in previous experiments,[12,13] we have purposely oxidized a sample by exposure to air for a period of one week. In agreement with other photo-oxidation studies,[14,22] the oxidized films exhibit a PA feature that dramatically reduced the SE.[25]

B. Interaction dynamics

With increasing pump irradiance and, hence, increasing excitation densities in the MEH-PPV film, the initial decay rates of the SE and PA become faster and dependent on the excitation density. In Fig. 4 the dynamics of the SE (probed at 632 nm) are shown for increasing excitation densities of 3.6×10^{18} cm^{-3} (squares), 1.2×10^{19} cm^{-3} (triangles), and 2.9×10^{19} cm^{-3} (circles). Throughout this paper, the numbers quoted for excitation density are the maximum values, i.e., at the front surface of the sample. The highest excitation density is still well below the threshold for gain narrowing for these MEH-PPV films;[27] thus, the fast decay at high densities is not due to amplified stimulated emission. The sym-

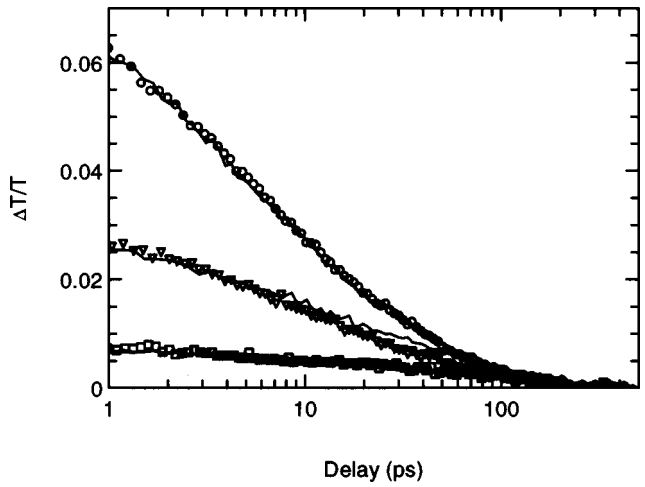

FIG. 4. SE differential transmittance for MEH-PPV film pumped at 450 nm with an excitation density at the front of the sample of 3.6×10^{18} cm^{-3} (squares), 1.2×10^{19} cm^{-3} (triangles), and 2.9×10^{19} cm^{-3} (circles). Lines show the same for pumping at 545 nm.

bols in Fig. 4 show the SE data obtained when the MEH-PPV film was pumped at 450 nm, while the solid lines represent data obtained when pumping at 545 nm. The fact that the noninteracting excitations (i.e., at low excitation densities, Fig. 3) and the interacting excitations (at high excitation densities, Fig. 4) show decay dynamics that are independent of the pump wavelength proves that the state responsible for the SE and PA is the same no matter how the primary excitation was formed, at least while pumping within the visible absorption band.

In order to study the effect of interactions between excitations on the decay dynamics, we examine time-delayed pump-probe data in the spectral ranges associated with PA and SE. Figure 5(a) shows the decay dynamics of PA, probed at 775 nm and pumped at 490 nm, analogous to the SE data in Fig. 4. In Fig. 5(a), we plot the normalized differential transmittance (normalized to its value at $t=0$) to better illustrate that at higher pump energies, the excitations decay more rapidly. From the decay dynamics of the PA [Fig. 5(a)] and the SE, we find that the effect of bimolecular interactions can be seen when the excitation density at the front surface ($N_0=\alpha F/\hbar\omega$, where F is the input fluence and α is the linear absorption coefficient at frequency ω) is above 2×10^{18} cm^{-3}. There are reports of interaction at even lower excitation levels (e.g., $N_0\approx3\times10^{17}$ cm^{-3}).[18] This implies significant interaction between excitations even at a mean separation of 10 nm, as calculated directly from the concentration, assuming a random distribution of excitations. This relatively long distance suggests that the interaction takes place between excited species from different chains (interchain interaction).

The same study performed on solutions of MEH-PPV shows no change in the dynamics with varying the pump fluence; in the solution both SE and PA had the same dynamics when the excitation density was varied from 10^{15} to 10^{17} cm^{-3}. Thus, in solution, when the polymer chains are dilute and well separated, there is no indication of bimolecular decay dynamics. Because the optical densities of solution and film samples were almost the same, and because we used

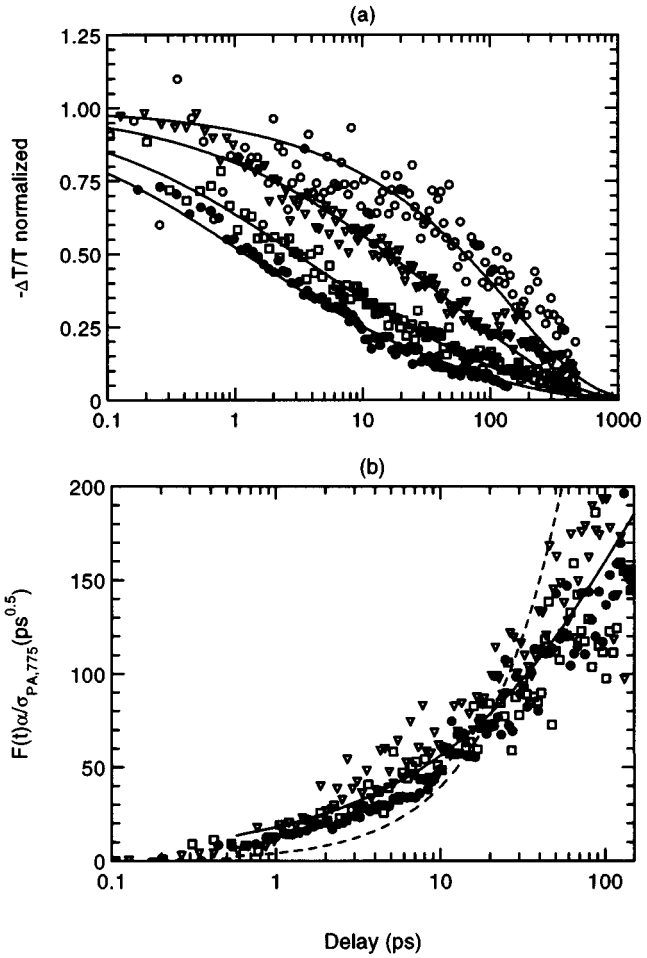

FIG. 5. PA differential transmittance for MEH-PPV, normalized (a), and transformed as described in text (b) to yield the interaction dynamics, for excitation densities of 1.4×10^{18} cm^{-3} (open circles), 4×10^{18} cm^{-3} (triangles), 1.0×10^{19} cm^{-3} (squares), and 1.6×10^{19} cm^{-3} (closed circles). The lines are best fits with $\beta/\sqrt{I}$ (solid lines) and constant β (dashed line) for $f(t)$ (see text).

the same fluence range for the pump beam, the number of excitations per chain was comparable in film and solution. Thus, the bimolecular decay observed in solid films arises predominantly from interactions between excitations on different macromolecular chains.

Because of the bimolecular interactions, the decay rate (in the absence of interaction, the inverse of the natural lifetime) becomes density dependent. This leads to the addition of a quadratic term in the description of the decay of the excitation density after the pump pulse:[17,28]

$$\frac{dN}{dt}=-\frac{N}{\tau}-f(t)N^2, \tag{3}$$

where $f(t)$ characterizes the interaction between the excitations and τ is the natural lifetime. For simplicity, we will assume from now on a single exponential decay at low excitation densities. This assumption does not affect the interpretation of the interaction dynamics for two reasons: first, a single exponential decay provides a reasonably accurate description of the data (because of the small contribution of the fast decay), and second, the faster initial contribution to the decay (at low excitation densities) is quickly hidden by the

faster bimolecular contribution at high densities. The rapid decay resulting from interactions between excitations has been studied assuming a constant coefficient of the quadratic term in the rate equation[20] or a coefficient proportional to $1/\sqrt{t}$.[17] We will attempt to determine the time dependence of $f(t)$ directly from fits to the data. For this purpose, we transform the pump-probe data by introducing a new variable, given by

$$y(t)=e^{-t/\tau}/N(t), \tag{4}$$

where $N(t)$ is obtained from the differential transmission data and τ is the natural lifetime (in the absence of the interaction). From Eq. (3), the rate equation for $y(t)$ becomes $dy/dt=f(t)e^{-t/\tau}$. This means that by plotting the derivative of Eq. (4), one can directly obtain the time dependence of the coefficient of the quadratic term $f(t)$. Because of the noise in the data this approach proves to be cumbersome. We can, however, extract the integral of $f(t)$ directly from the data in the form given by Eq. (4):

$$y(t)=e^{-t/\tau}/N(t)=1/N(0)+\int_0^t f(t')e^{-t'/\tau}dt'. \tag{5}$$

Equation (5) shows that by plotting the data in terms of the new variable, one should obtain the same time dynamics for all the curves because the time dependent part of the right-hand side, $F(t)=\int_0^t f(t')e^{-t'/\tau}dt'$, does not depend on the initial excitation density $N(0)$. The data in Fig. 5 prove that this is indeed true. The symbols in Fig. 5(b) represent the pump-probe data from Fig. 5(a) replotted after applying Eq. (5) to the differential change in transmittance.

It is straightforward to show that for small signals (few percent)

$$\frac{\Delta T}{T}(0)=\frac{\sigma(1-e^{-\alpha L})}{\alpha}N_0\cong\frac{\sigma N_0}{\alpha}, \tag{6}$$

where α is the linear absorption coefficient, σ is the cross section for the excited-state process (SE or PA), and N_0 is the highest excitation density (at the front surface of the sample). From this, we calculate $\sigma_{\mathrm{SE},632}=6.3\times10^{-16}$ cm^2 and $\sigma_{\mathrm{PA},775}=2.1\times10^{-16}$ cm^2 for the stimulated emission and photoinduced absorption cross sections, respectively. The approximation made in Eq. (6) is valid because of the high optical density of the MEH-PPV samples at all the pump wavelengths, $\exp(-\alpha L)\leqslant0.03$. Equation (6) shows that all the equations that apply for N can be used for $\Delta T/T$ as well. We note that the initial excitation density (the initial photoinduced signal) is linear with the input pump energy even at densities that indicate strong interaction (i.e., signals over 10%). This provides confidence that there are no higher order nonlinearities (e.g., further excitation to a higher excited state or excitation of a biexciton). In the case of biexciton formation, the signals at zero delay are proportional to the square of the pump intensity (and not linear).[22,24] In this work, measurements of the dynamics were restricted to pump powers below the regime of biexciton formation (defined by an input fluence greater than 3.1 mJ/cm^2 for methyl-substituted ladder-type poly(*para*-phenylene) (m-LPPP) (Ref. 24) or greater than 0.6 mJ/cm^2 for MEH oligomers[23]). Given that the absorption coefficient is above 10^4 cm^{-1}, the excitation density in the biexciton studies was more than 2×10^{19} cm^{-3}. By performing experiments in thicker (500 nm) films, we were able to measure the dynamics of the excited state below 10^{19} cm^{-3}, which corresponds to input fluences between 0.5 μJ/cm^2 and 50 μJ/cm^2. The observation that both the SE and PA signals immediately after zero delay are linear in input fluence implies that the two-exciton formation does not influence the dynamics.

In Fig. 5(b), we have subtracted the constant factor $1/[\Delta T/T(0)]$, proportional to $1/N(0)$, from each curve. By fitting the data in this form we directly obtain the time dependence of $F(t)$, the integral form of $f(t)$. The fact that all the curves in Fig. 5(b) show the same dynamics, although as shown in Fig. 5(a) they clearly decay differently, indicates that a rate equation of the form given by Eq. (3) is appropriate. The solid line in Fig. 5(b) represents a fit to the data assuming that $f(t)=\beta/\sqrt{t}$, which means $F(t)=\sqrt{2\pi\tau}\beta\ \mathrm{erf}(\sqrt{t/\tau})$, where β is a constant and $\mathrm{erf}(x)=2/\sqrt{\pi}\int_0^\infty \exp(-x^2)dx$ is the error function. The dashed line represents the best fit with $f(t)=\beta'$, which gives $F(t)=\beta'\tau(1-e^{-t/\tau})$. As indicated in Fig. 5(b), a $1/\sqrt{t}$ time dependence provides a better description of the data than a constant for the function $f(t)$. Analysis of both the PA and SE lead to the same conclusion. By fitting several data sets [including the solid lines in Fig. 5(a)] and using Eq. (6), we found

$$f(t)=\beta/\sqrt{t} \tag{7}$$

with $\beta=2\times10^{-20}$ cm$^3/\sqrt{\mathrm{ps}}$. This value for β is twice that reported by Maniloff, Klimov, and McBranch for a PPV oligomer.[17] The other fit [dashed line in Fig. 5(b)] obtained by using a constant coefficient of the quadratic term for Eq. (3) yields $\beta'=1.1\times10^{-20}$ cm^3/ps, the same order of magnitude as that reported for PPV.[20,21]

IV. DISCUSSION OF INTERACTION MECHANISMS

The physical interpretation of Eq. (3) is that two excitations disappear as a result of the interaction between them (e.g., exciton-exciton annihilation or exciton fusion with creation of a higher energy excited state[29]). Here we discuss the mechanisms leading to this interaction process.

There are two independent experimental facts.

(1) Bimolecular decay is observed. The coefficient of the bimolecular decay term is given by Eq. (7) with $\beta=2\times10^{-20}$ cm$^3/\sqrt{\mathrm{ps}}$.

(2) The range of the interaction which leads to the bimolecular decay is at least 10 nm in the picosecond regime.

The mechanism responsible for the bimolecular decay must be consistent with both (1) and (2).

Excitation transfer via the dipole-dipole interaction, known as the Förster energy-transfer process, has been well studied.[28,30–34] In addition, excitations can interact with one another through classical diffusion. Finally, quantum delocalization provides a mechanism for long-range interaction. In the following, we briefly consider the contributions from these mechanisms for bimolecular interaction.

A. Long-range dipole-dipole interaction (Refs. 30–33 and 35)

The dipole-dipole interaction leads to a $1/\sqrt{t}$ dependence for the coefficient of the bimolecular interaction term in the rate equation. In this case, Eqs. (3) and (7) are correct with the coefficient β given by

$$\beta = \frac{1}{2}\,\frac{4\pi R_0^3}{3}\,\sqrt{\pi/\tau}, \tag{8}$$

where R_0 is the distance between the dipoles at which the decay rate due to the interaction equals the natural decay given by $1/\tau$. The contribution to the bimolecular decay rate from Förster transfer is $(R_0/R)^6/\tau$, which means that $4\pi R_0^3/3$ defines the dipole-dipole interaction volume; at distances longer than R_0, $(R_0/R)^6/\tau < 1/\tau$, the bimolecular decay via Förster transfer is ineffective. From Eq. (8) and the measured value of β, we obtain $R_0 \cong 4.5$ nm. However, this value for R_0 is not consistent with the measured range. In order for the Förster dipole-dipole interaction to account for the measured range ($\geqslant 10$ nm), the measured β would have to be an order of magnitude larger ($2^3 = 8$). Nevertheless, the dipole-dipole interaction leads to the correct time dependence for the decay and contributes to the bimolecular decay.

The effective range can be extended in two ways: through classical diffusion of the excitations, provided the diffusion constant is large enough to enable diffusion over distances of approximately 5 nm in the picosecond regime, and through quantum delocalization.

B. Diffusion of excitations

Diffusion yields the following expression for the coefficient of the quadratic term in the rate equation:[28,36]

$$f(t) = 4\pi DR\left(1 + \frac{R}{\sqrt{\pi Dt}}\right), \tag{9}$$

where D is the diffusion constant and R is the encounter distance (the distance between the excitations at the moment of interaction). Two distinct regimes are evident from Eq. (9): (i) the high-diffusion limit where $D > R^2/(\pi t)$ and $f(t) \cong 4\pi DR$; (ii) the low-diffusion limit where $D < R^2/(\pi t)$ and $f(t) = \beta/\sqrt{t}$. In both cases, the picosecond regime is the relevant time scale, for the effect of bimolecular decay is clearly seen at 1 ps [see Fig. 5(a)].

In the high-diffusion limit, the coefficient of the interaction term in Eq. (3) is a constant. Although a constant term does not fit the data as well as the square-root dependence of Eq. (7) (see Fig. 5), using the ''best-fit'' value for β' [Fig. 5(b), dashed line] and assuming $R \approx 5$ nm yields $D \approx 1.7 \times 10^{-3}$ cm^2/s. This value is an upper limit for the diffusion coefficient because we have assumed that all the measured bimolecular decay rate is due to diffusion. Such a small value for the diffusion constant would be inconsistent with the inequality (i) defining the high-diffusion regime, which implies that the typical distance traveled by an excitation in 1 ps, $r < (Dt)^{1/2} \approx 0.5$ nm, would be far too small to account for the measured interaction range (at least 5 nm until the dipole-dipole interaction can contribute).

The low-diffusion limit leads to the same time dependence as in Eq. (7) and suggested by our experimental data, with a coefficient $\beta = 4\sqrt{\pi D}R^2$. In this limit, however, D would be even smaller (of the order 10^{-4} cm^2/s). Again, therefore, the typical distance traveled by an excitation in 1 ps would be far too small to make a significant contribution to the decay. We conclude that diffusion of excitations is not of major importance to the bimolecular decay in the picosecond regime, although it may play a role in the bimolecular dynamics at longer times (e.g., after 100 ps, when the bimolecular contribution becomes very small).

C. Quantum delocalization

The dipole-dipole interaction is not effective at distances above 5 nm, and diffusion is too slow to contribute in a significant way to the bimolecular decay in the picosecond regime. Therefore, in order to explain the observed interaction between excitations at distances larger than 10 nm, the wave function of the photoexcitation must be delocalized over a distance of at least 5 nm.

We have seen that the dipole-dipole interaction between localized excitations leads to a time-dependent bimolecular decay rate [as given by Eqs. (7) and (8), and indicated by the data in Fig. 5]. The fact that the bimolecular decay rate decreases with time arises from the strong distance dependence of the dipole-dipole interaction: at longer times, the coefficient of the bimolecular term decreases (as $1/\sqrt{t}$) because the nearer neighbors are depleted as time progresses. This local depletion effect is in addition to the average concentration dependence of the bimolecular interaction, given by the square of the concentration in the rate equation. In the case of completely delocalized excitations, Eq. (3) would have a constant bimolecular decay rate [i.e., $f(t)$ is constant], suggesting a somewhat softer time dependence than $1/\sqrt{t}$ (consistent with the data shown in Fig. 5). The true picture involves quantum delocalization over about 5 nm. Unfortunately, the time dependence of $f(t)$ is not known for bimolecular interaction between quantum delocalized excitons. On physical grounds, we expect the same local depletion effect to be operative; however, the detailed time dependence will depend on the form of the spatial decay of the delocalized wave function.

A quantum delocalization distance greater than 5 nm as required by the measured range is roughly consistent with recent calculations by Köhler *et al.*[37] who predict that the excitations created by pumping into the main visible absorption band result from transitions between orbitals delocalized over approximately 5 monomer units, or about 4 nm. We note, however, that the interchain nature of the bimolecular interactions was not considered by Köhler *et al.*

The bimolecular decay arises from interchain interactions; it is not observed in solutions under the same excitation densities, i.e., same density-per-chain of excitations. Thus, since an average delocalization of 5 nm is needed to explain the dynamics, the data suggest that the wave function of the excitations extends over several chains [the distance between two chains in MEH-PPV film cast from the THF solution is known to be less than 0.4 nm (Ref. 38)]. However, the exact shape of the three-dimensional wave function cannot be inferred from our experiments. Although interaction between excited species on the same chain is possible, we estimate the distance between two intrachain excited species to be

more than 1000 monomer units at an excitation density of 10^{18} cm^{-3}. We are currently performing studies on highly oriented films in order to obtain better insight in this problem.

V. CONCLUSION

In summary, we have examined the temporal and spectral behavior of the excitations in MEH-PPV during the lifetime of the emitted PL. The magnitude and decay of the SE and PA probed at 632 and 775 nm, respectively, do not change when the pump wavelength varies within the visible absorption band. We have carefully analyzed the interchain bimolecular interaction that shortens the decay for both SE and PA (and, implicitly, PL). The observation of bimolecular decay even in the picosecond regime is inconsistent with diffusion over large distances. Explaining the magnitude of the bimolecular decay dynamics with a combination of the dipole-dipole interaction (Förster energy transfer) plus diffusion leads to a range of only 4.5 nm. Thus, to account for the measured range, as determined from the onset of bimolecular decay as a function of excitation density, the excitations must be delocalized well beyond a single chain, with wave function that extends over about 5 nm.

ACKNOWLEDGMENTS

This research was supported by the National Science Foundation under Contract No. DMR95-10387 and by the Los Alamos National Laboratory (Contract No. STB/UC: 96-136).

[1] J. H. Burroughes, D. D. C. Bradley, A. R. Brown, R. N. Marks, K. Mackay, R. H. Friend, P. L. Burns, and A. B. Holmes, Nature (London) **347**, 539 (1990).
[2] D. Braun and A. J. Heeger, Appl. Phys. Lett. **58**, 1982 (1991).
[3] Q. Pei, G. Yu, C. Zhang, Y. Yang, and A. J. Heeger, Science **269**, 1086 (1995).
[4] G. Yu, J. Gao, J. C. Hummelen, F. Wudl, and A. J. Heeger, Science **270**, 1789 (1995).
[5] N. Tessler, G. J. Denton, and R. H. Friend, Nature (London) **382**, 695 (1996).
[6] F. Hide, M. A. Diaz-Garcia, B. J. Schwartz, M. R. Andersson, Q. Pei, and A. J. Heeger, Science **273**, 1833 (1996).
[7] S. V. Frolov, W. Gellermann, M. Ozaki, K. Yoshino, and Z. V. Vardeny, Phys. Rev. Lett. **78**, 729 (1997).
[8] J.-L. Bredas, J. Cornil, and A. J. Heeger, Adv. Mater. **8**, 447 (1996).
[9] I. H. Campbell, T. W. Hagler, D. L. Smith, and J. P. Ferraris, Phys. Rev. Lett. **76**, 1900 (1996).
[10] J. M. Leng, S. Jeglinski, X. Wei, R. E. Brenner, and Z. V. Vardeny, Phys. Rev. Lett. **72**, 156 (1994).
[11] M. Chandross and S. Mazumdar, Phys. Rev. B **55**, 1497 (1997).
[12] M. Yan, L. J. Rothberg, F. Papadimitrakopoulos, M. E. Galvin, and T. M. Miller, Phys. Rev. Lett. **72**, 1104 (1994).
[13] M. Yan, L. J. Rothberg, E. W. Kwock, and T. M. Miller, Phys. Rev. Lett. **75**, 1992 (1995).
[14] L. J. Rothberg, M. Yan, F. Papadimitralopoulos, M. E. Gavin, E. W. Kwock, and T. M. Miller, Synth. Met. **80**, 41 (1996).
[15] I. D. W. Samuel, G. Rumbles, C. J. Collison, R. H. Friend, S. C. Moratti, and A. B. Holmes, Synth. Met. **84**, 497 (1997).
[16] N. T. Harrison, G. R. Hayes, R. T. Phillips, and R. H. Friend, Phys. Rev. Lett. **77**, 1881 (1996).
[17] E. S. Maniloff, V. I. Klimov, and D. W. McBranch, Phys. Rev. B **56**, 1876 (1997).
[18] J. Z. Zhang, M. A. Kreger, G. Klaerner, M. Kreyenschmidt, R. D. Miller, and J. C. Scott, Proc. SPIE **3145**, 363 (1997).
[19] D. Vacar, A. Dogariu, and A. J. Heeger, Adv. Mater. **10**, 669 (1998).
[20] R. G. Kepler, V. S. Valencia, S. J. Jacobs, and J. J. McNamara, Synth. Met. **78**, 227 (1996).
[21] N. Tessler, G. J. Denton, N. T. Harrison, M. A. Stevens, S. E. Burns, and R. H. Friend, Synth. Met. **91**, 61 (1997).
[22] V. I. Klimov, D. W. McBranch, N. N. Barashkov, and J. P. Ferraris, Chem. Phys. Lett. **277**, 109 (1997).
[23] V. I. Klimov, D. W. McBranch, N. Barashkov, and J. Ferraris, Phys. Rev. B (to be published).
[24] G. Kranzelbinder, M. Nisoli, S. Stagira, S. D. Silvestri, G. Lanzani, K. Mullen, U. Scherf, W. Graupner, and G. Leising, Appl. Phys. Lett. **71**, 2725 (1997).
[25] D. Vacar, A. Dogariu, and A. J. Heeger, Chem. Phys. Lett. **290**, 58 (1998).
[26] A. Dogariu and A. J. Heeger (unpublished).
[27] The sapphire substrate prevents wave guiding, and the gain coefficients are much less than unity.
[28] R. C. Powell and Z. G. Soos, J. Lumin. **11**, 1 (1975).
[29] M. Pope and C. E. Swenberg, *Electronic Processes in Organic Crystals* (Clarendon, Oxford, 1982).
[30] T. Forster, Ann. Phys. (Leipzig) **2**, 55 (1948).
[31] T. Forster, Z. Naturforsch. A **4a**, 321 (1949).
[32] T. Forster, Discuss. Faraday Soc. **27**, 7 (1959).
[33] T. Forster, in *Modern Quantum Chemistry, Istanbul Lectures*, edited by O. Sinanoglu (Academic, New York, 1965), Vol. III, p. 93.
[34] R. C. Powell and R. G. Kepler, *Molecular Crystals and Liquid Crystals* (Gordon and Breach, New York, 1970), Vol. 11, p. 349.
[35] K. B. Eisenthal and S. Siegel, J. Chem. Phys. **41**, 652 (1964).
[36] S. Rice, in *Comprehensive Chemical Kinetics*, edited by C. H. Bamford, C. F. H. Tipper, and R. G. Compton (Elsevier, Amsterdam, 1985), Vol. 25.
[37] A. Kohler, D. A. d. Santos, D. Beljonne, Z. Shuai, J.-L. Bredas, A. B. Holmes, A. Kraus, K. Mullen, and R. H. Friend, Nature (London) **392**, 903 (1998).
[38] C. Y. Yang, F. Hide, M. A. Diaz-Garcia, A. J. Heeger, and Y. Cao, Polymer **39**, 2299 (1997).